Reinforcing effect of polyurea resin coating on RC members subject to low-speed and medium-speed impact

Sonoda, Yoshimi
Department of Civil Engineering, Kyushu University

Tamai, Hiroki
Department of Civil Engineering, Kyushu University

Ifuku, Tatsuya
Department of Civil Engineering, Kyushu University

Koshiishi, Masami
Nippon Koei Co.,Ltd.

https://hdl.handle.net/2324/7170248

KYUSHU UNIVERSITY

Reinforcing effect of polyurea resin coating on RC members

subject to low-speed and medium-speed impact

Yoshimi Sonoda, Hiroki Tamai, Tatsuya Ifuku, Masami Koshiishi

Abstract

Polyurea resin is widely used as a coating material for civil engineering structures due to their relatively high strength and elongation ability and its applications for improving the impact resistance and explosion resistance of concrete and steel structures have also been studied. However, the reinforcing effect against lower-speed impact loads has not been well studied. In this study, we investigated the load-bearing capacity of RC structural members coated with polyurea resin under repeated impact loads using a low-speed falling weight and a medium-speed flying object. The results of low-speed repeated impact test showed that there was no significant effect under the first impact, however, when the number of impacts increased, the strengthening effect of the polyurea resin was confirmed. In addition, by coating the back side of the RC slab, the remarkable effect of preventing the scattering of concrete pieces was verified in the medium-speed repeated impact test. In this study, Finite element simulations of these two types of impacts were performed, and the strengthening effect of polyurea resin was analyzed and the same tendencies as impact tests were reproduced.

1   Introduction

Polyurea resin has relatively high strength and elongation ability, as well as excellent water retention, abrasion resistance, chemical resistance, and impact resistance; thus, it is widely used as a coating material for various civil engineering structures [1]–[6]. Recently, applications for improving the impact resistance and explosion resistance of concrete and steel structures have also been studied [7]–[14].

For example, Amin et al. [7] investigated the impact response of a steel sheet coated with polyurea resin using a direct pressure pulse test and confirmed the improved impact resistance of the steel sheet due to the coating. A numerical simulation study to investigate the impact resistance of steel plate with polyurea resin coating was conducted by Samiee et al. [8], and the dynamic response of steel plates coated with polyurea resin under low-speed impact was studied by Jiang et al. [9].

As regards extant research on concrete structural members coated with polyurea resin, an experimental

31 study on the explosion resistance of concrete slabs reinforced on the back side with polyurea resin was

32 performed by Ichino et al. [12]. Further, a three-point bending test and an explosion experiment were

33 conducted on a concrete panel coated with polyurea resin and carbon fiber reinforced plastics (CFRPs) by

34 Chen et al. [13]. They reported that concrete panels reinforced with polyurea resin have better load-bearing

35 performance against explosive loads than panels reinforced with CFRP but are less resistant to static load.

36 Ha et al. [14] proposed a new composite material that combines CFRP, which is a high-rigidity and high-

37 strength material, and polyurea, which is a high-ductility material. They coated a reinforced concrete (RC)

38 slab with the composite material, investigated the explosion resistance of the coated, and confirmed its

39 effectiveness.

40 Polyurea resins are generally recognized to have a clear reinforcing effect when coated on surfaces

41 subject to high-speed impact and explosion loads. However, the reinforcing effect against lower-speed

42 impact loads has not been well studied. In addition, research concerning numerical simulation of RC

43 members coated with polyurea resin under low-speed or medium-speed impact has been scarce.

44 In this study, we investigated the load-bearing capacity of RC structural members coated with polyurea

45 resin using impact tests and numerical simulations. In particular, repeated impact tests of an RC cantilever

46 beam with low-speed falling weight, and repeated impact tests of an RC slab with a medium-speed flying

47 object were conducted, to elucidate the fracture process of RC structural members coated with polyurea

48 resin. Furthermore, finite element (FE) simulations of these two types of impacts were performed, and the

49 strengthening effect of polyurea resin was analyzed on the basis of the numerical analysis results.

50 ## 2 <u>**Low-speed repeated impact test of RC cantilever**</u>

51

52 To examine the response to low-velocity impact loads of RC members coated with polyurea resin, a

53 repeated weight drop impact test was conducted on RC cantilever beams.

54

55 ### 2.1 <u>**Experiment outline**</u>

56 Figure 2.1 shows a schematic diagram of the test specimen. The RC cantilever beam specimen has a

57 length of 1000 mm and a cross-sectional dimension of 600 mm × 200 mm (width × height), and D10

58 (SD345) is placed as the main reinforcing bar and shear reinforcing bar. The polyurea resin was applied

59 uniformly to the upper and lower surfaces of the beam, the upper surface of the footing, and the side surfaces,

60 with a thickness of 2 mm. Photo 2.1 shows the drop-weight impact test device. Photo 2.2 shows the shape

61 of the weight, and Table 2.1 shows the loading conditions. The experiment was carried out by freely

62 dropping a weight with a mass of 1000 kg from a predetermined height and repeatedly colliding with the

63 specimen. The initial drop was performed from a height of 300 mm, after which five drops were performed

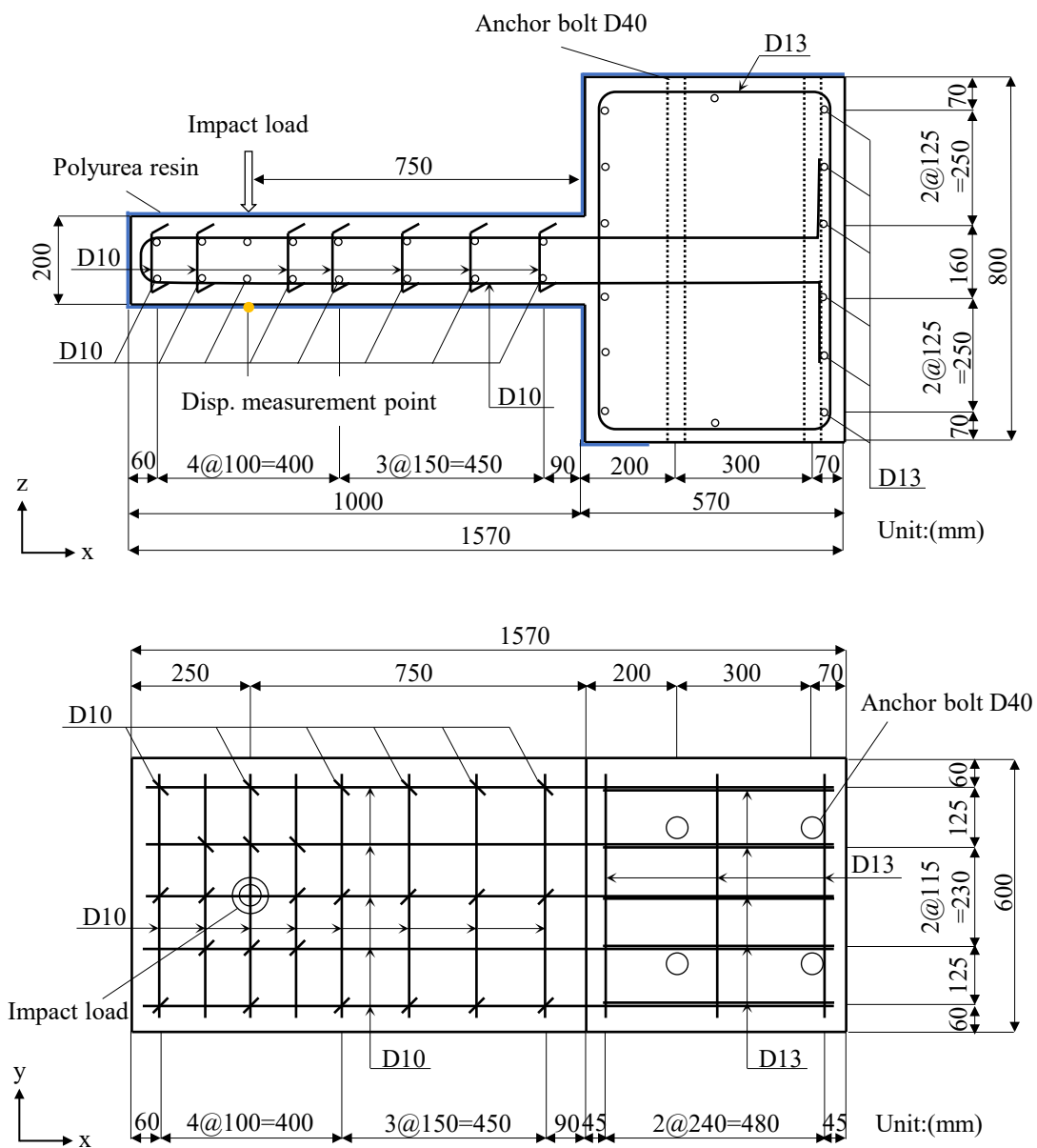64 at each of 50, 100, 150 and 200mm.

Anchor bolt D40

Impact load

Polyurea resin

750

D10

200

D10

Disp. measurement point

D10

D10

D13

2@125 =250

160

2@125 =250

70

70

800

z

x

60

4@100=400

3@150=450

90

200

300

70

1000

570

1570

D13

Unit:(mm)

1570

250

750

200

300

70

D10

Anchor bolt D40

60

125

2@115 =230

125

60

600

D13

D10

Impact load

D10

D13

y

x

60

4@100=400

3@150=450

90

45

2@240=480

45

Unit:(mm)

Figure 2.1 Schematic diagram of the test specimen
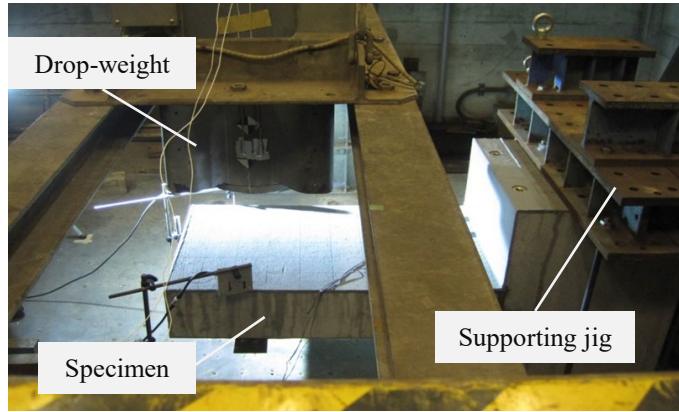
Photo 2.1 Drop-weight impact test device   Photo-2.2 Shape of weight
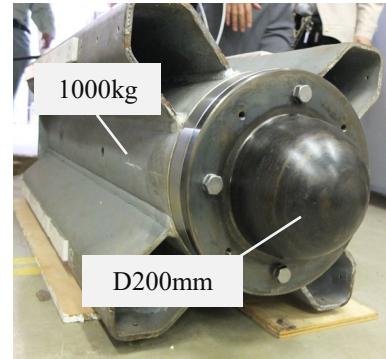
Table 2.1 Loading condition

Impact Number	1	2—6	7—11	12—16	17
Drop Height (mm)	300	50	100	150	200
Impact Velocity (m/sec)	2.43	0.99	1.4	1.72	1.98

65

66 ## 2.2 **Experimental results and discussion**

67 Figure 2.2 shows the displacement response at the first impact, and Figure 2.3 shows the relationship

68 between the number of impacts and maximum displacement. In the first impact loading, there was almost

69 no difference in displacement response. However, as the number of impacts increased, the displacement of

70 the specimen coated with polyurea decreased more than that of the specimen without the coating.

71 Furthermore, the specimen without polyurea coating collapsed as the five tension-side main reinforcing

72 bars ruptured at the 11th impact loading. In contrast, the specimen with polyurea coating did not collapse

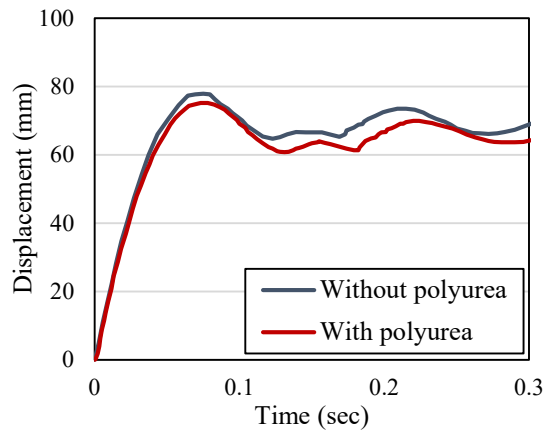73 completely until the 17th impact loading.
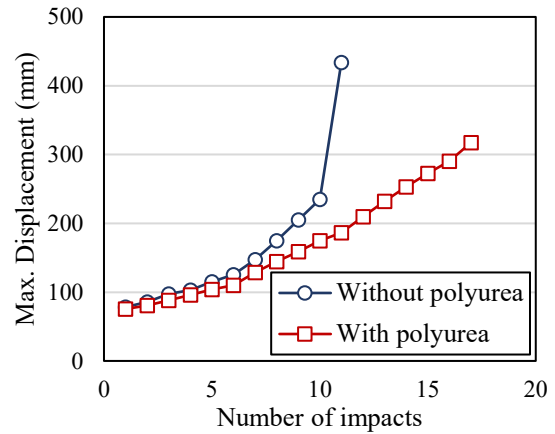
Figure 2.2 Displacement response at the first impact

Figure 2.3 Relationship between the number of impacts and maximum displacement

(a) Specimen without polyurea coating

(after 11th impact)

(b) Specimen with polyurea coating

(after 17th impact)

Photo 2.3 Failure status

74

75   Photos 2.3 (a) and (b) show the state of collapse of the specimens. In the specimen without polyurea

76   coating, large cracks occurred from the upper edge of the beam base, and the concrete on the compression

77   side of the beam base were crushed, causing concrete pieces to peel off. Conversely, in the specimen coated

78   with polyurea, even after the polyurea resin was peeled off at the beam base, the resin held the footing

79   foundation and the beam member together and exerted a restoring force. It was also found that the crushed

80 concrete could be prevented from peeling off on the compression side of the beam base. These results

81 confirmed that by coating with polyurea resin, the impact absorption performance can be improved by the

82 shape-retaining effect of the polyurea resin under a low-speed repeated impact load.

83

84 **3   Numerical simulations for low-speed repeated impact test of RC cantilever**

85

86 **3.1   Finite element model**

87   Figure 3.1 shows the FE model for the RC cantilever. In this analysis, a half-symmetry model was used.

88 Concrete and polyurea resin are modeled using three-dimensional solid elements, and steel bars are

89 modeled by embedded steel truss elements.

(a) RC cantilever with polyurea coating   (b) Steel reinforcement
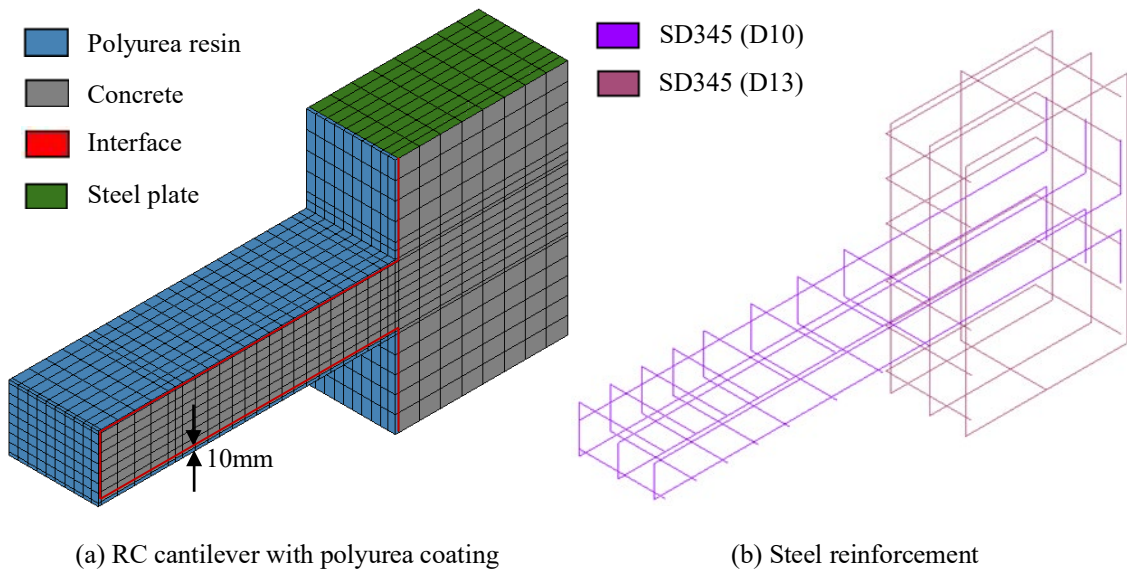
Figure 3.1 Finite element model for RC cantilever

90   This analysis reproduces an experiment in which the impact is repeated 10 times or more. Therefore, if

91 the entire model is divided into fine meshes and the number of elements increases, the calculation cost will

92 also increase. Therefore, the concrete element with a size of about 10 to 50 mm is used in this study. Along

93 with this, though the actual polyurea resin is coated on the beam with a thickness of 2 mm, in the analysis

94 model, it is modeled with a thickness of 10 mm so that the aspect ratio of the polyurea resin element does

95 not become large. In addition, to avoid overestimating stiffness at five times the actual element thickness,

96 we used corrected Young's modulus which is divided by the rate of increase in thickness.

97

98 ## 3.2   Physical properties

99   Table 3.1 shows the physical properties of each material. The values obtained by the material tests are

100 mainly used. The Young's modulus and density of the polyurea resin are also given after the reduction

101 described in the previous section. The Poisson's ratio of the polyurea resin follows that of Parniani et al.

102 [15].

103   A rotationally distributed cracking model was used for the concrete. Figure 3.2 shows the assumed

104 stress-strain relationship. For the compression side, a compression softening model was applied, based on

105 the *Concrete Standard Specification* of the JSCE [16], as formulated by Equations (3.1)–(3.4).

106
$$\sigma_c = E_0 K(\varepsilon - \varepsilon_p) \tag{3.1}$$

107
$$E_0 = 2f'_{ck}/\varepsilon_c \tag{3.2}$$

108
$$K = exp\left\{-0.73\frac{\varepsilon}{\varepsilon_c}\left(1 - exp\left(-1.25\frac{\varepsilon}{\varepsilon_c}\right)\right)\right\} \tag{3.3}$$

109
$$\varepsilon_p = \varepsilon_c - 2.86 \cdot \varepsilon_c\left\{1 - exp\left(-0.35\frac{\varepsilon}{\varepsilon_c}\right)\right\} \tag{3.4}$$

110 where σ_c is the compressive stress (N/mm²), f'_{ck} is the compressive strength (N/mm²), ε is the total

111 strain, ε_c is the strain at compressive strength, E_0 is the initial stiffness (N/mm²), ε_p is the plastic strain,

112 and K is the modulus of the elastic stiffness residual rate.

Table 3.1 Physical properties

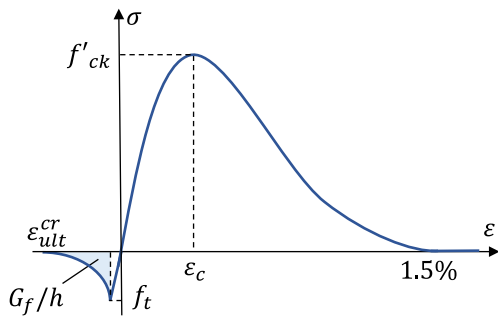| Material	Mass density [kg/m³]	Young's modulus [GPa]	Poisson's ratio	Strength [MPa]
Steel	7850.8	186.5	0.3	394.1(yield), 574.5(ultimate)
Concrete	2320	29.5	0.2	25.1(compressive), 1.97(tensile)
Polyurea resin	1000 (200)	0.11 (0.02)	0.26	24.0

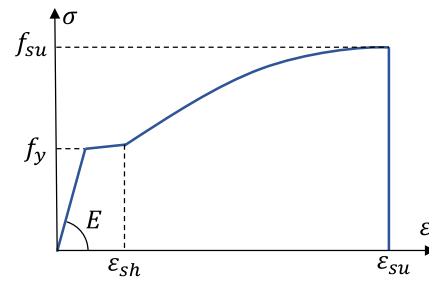Figure 3.2 Stress-strain relationship of concrete

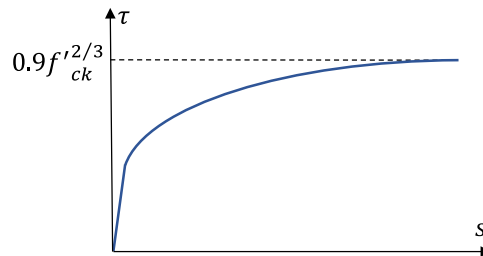Figure 3.3 Stress-strain relationship of steel

Figure 3.4 Adhesion stress-slip relationship between concrete and reinforcing bar

113

114   For the tensile side, a linear elastic material was assumed up to the tensile strength, and after the tensile

115   strength, the Hordijk model [17] given by Equations (3.5) and (3.6) was applied. The tensile strength and

116   fracture energy were calculated using Equations (3.7) and (3.8) in reference to the *Concrete Standard*

117   *Specification* of the JSCE [16].

118
$$\frac{\sigma^{cr}\varepsilon^{cr}}{f_t} = \left(1 + \left(c_1\frac{\varepsilon^{cr}}{\varepsilon^{cr}_{ult}}\right)^3\right)exp\left(-c_2\frac{\varepsilon^{cr}}{\varepsilon^{cr}_{ult}}\right) - \frac{\varepsilon^{cr}}{\varepsilon^{cr}_{ult}}(1 + c_1^3)\,exp(-c_2) \tag{3.5}$$

119
$$c_1 = 3, \qquad c_2 = 6.93, \qquad \varepsilon^{cr}_{ult} = 5.136\frac{G_f}{h_{cr}f_t} \tag{3.6}$$

120
$$f_t = 0.23f'_{ck} \tag{3.7}$$

121
$$G_f = 10(d_{max})^{\frac{1}{3}} \cdot f'_{ck} \tag{3.8}$$

122 where σ^{cr} is the tensile stress, ε^{cr} is the cracking strain, ε^{cr}_{ult} is the ultimate cracking strain, h_{cr} is the

123 equivalent element length (mm), f_t is the tensile strength (N/mm²), G_f is the fracture energy (N/mm),

124 and d_{max} is the maximum size of the coarse aggregate (mm). Note that the equivalent element length h_{cr}

125 is the value of the cubic root of the element volume.

126 Figure 3.3 shows the stress-strain relationship assumed for the steel material. The Dodd-Restrepo model

127 [18] was used for the steel material model. This is a macroscopic model that predicts the cyclic stress-strain

128 behavior of reinforcing bars, and it can take into account both the Bauschinger effect and the fracture

129 behavior due to the reduction of stress when the fracture strain is reached. In Figure 3.3, f_y is the yield

130 strength (N/mm²), ε_{sh} is the strain at the beginning of hardening, f_{su} is the rupture strength (N/mm²), and

131 ε_{su} is the rupture strain.

132 The interface element at the interface between the concrete and the reinforcing bar introduces the

133 adhesion stress-slip relationship proposed by Shima et al. [19], which is shown in Figure 3.4 and Equation

134 (3.9). Note that linear elasticity is assumed in the normal direction of the interface element.

135
$$\tau = 0.9 \times f'_{ck}{}^{2/3}\left(1 - e^{-40\left(\frac{s}{D}\right)^{0.6}}\right) \tag{3.9}$$

136 where τ is the adhesion stress (N/mm²), s is the slip (mm), and D is the bar diameter (mm).

137 To investigate the material properties of polyurea resin, uniaxial tensile tests were conducted at a tensile

138 speed of 50 mm/min using the dumbbell test specimen shown in Figure 3.5 (a). Figure 3.5 (b) shows the

139 stress-strain relationship obtained from the uniaxial tensile tests.

(a) Dumbbell test specimen (b) Stress-strain relationship of polyurea resin
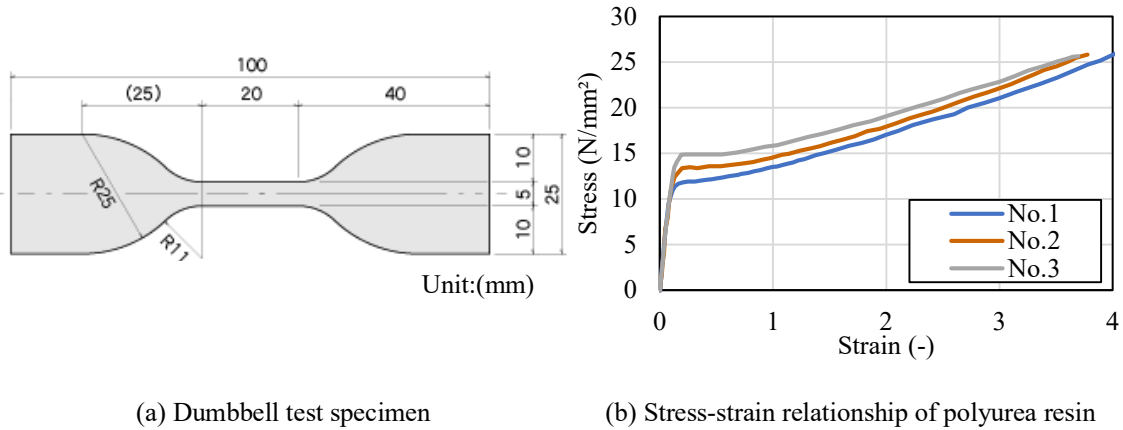
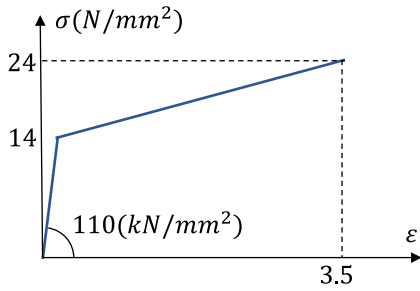Figure 3.5 Uniaxial tensile tests using the dumbbell test specimen

Figure 3.6 Stress-strain relationship of
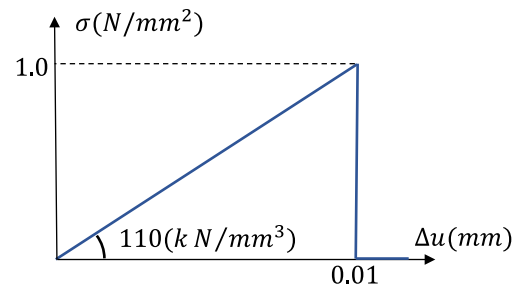
polyurea resin

Figure 3.7 Adhesion stress-relative displacement

relationship between polyurea resin and concrete

140

141   Several constitutive models have been proposed to describe the stress-strain behavior of polyurea resins.

142   Amirkhizi et al. [20] proposed an experimentally based linear viscoelastic constitutive model that

143   incorporated the classical Williams–Landel–Ferry (WLF) time-temperature transformation and pressure

144   response. Li et al. [21] proposed a hyper-viscoelastic constitutive model for polyurea resin that incorporates

145   the Ogden model and a nonlinear viscoelastic model. Zhang et al. [22] proposed a bilinear constitutive

146   model describing the temperature, strain rate, and pressure dependence of the stress-strain behavior.

147   However, many of the proposed constitutive models focus on the compressive characteristics of polyurea

148   resin, while a few have focused on the tensile characteristics. Furthermore, many of these constitutive

149   models are complex, which makes them difficult to apply. Therefore, the polyurea resin was assumed to be

150   a nonlinear elastoplastic material, and the stress-strain relationship shown in Figure 3.6 was assumed

151   because the focus of this study was on the tensile characteristics of the polyurea, and the basic investigation

152   of the coating effect was the objective of the analysis. Here, the unloading gradient of the polyurea resin is

153   equal to the initial stiffness, and residual strain is generated during unloading; therefore, the evaluation is

154   safer than when modeling as a hyper-elastic material.

155   An interface element is provided at the interface between the polyurea resin and the concrete, and the

156   adhesion stress-relative displacement relationship shown in Figure 3.7 is applied. Adhesion breaking was

157   expressed by setting the transfer force to zero when the stress generated in the interface element exceeded

158   the adhesion strength. Here, the initial stiffness of interface element is assumed as the stiffness of the

159   polyurea resin, which is the weaker stiffness material side, and the adhesion strength is 1.0 N/mm² based

160   on the results of the peeling test. The strain rate effect of each material was not considered, because the

161   purpose of the analysis in this study was not to reproduce the phenomenon accurately but to evaluate the

162   effect of polyurea resin coating by relative comparison.

163

3.3   Boundary condition

165   As shown in Figure 3.8, the boundary conditions were set to be the same as those in the experiment

166   described in Section 2.1. The bottom surface of the foundation is fixed in the triaxial direction, a steel plate

167   is installed on the top surface, and only the vertical direction of the plate is fixed. An interface element is

168   created at the interface between the plate and the foundation, and the force is transmitted only in the vertical
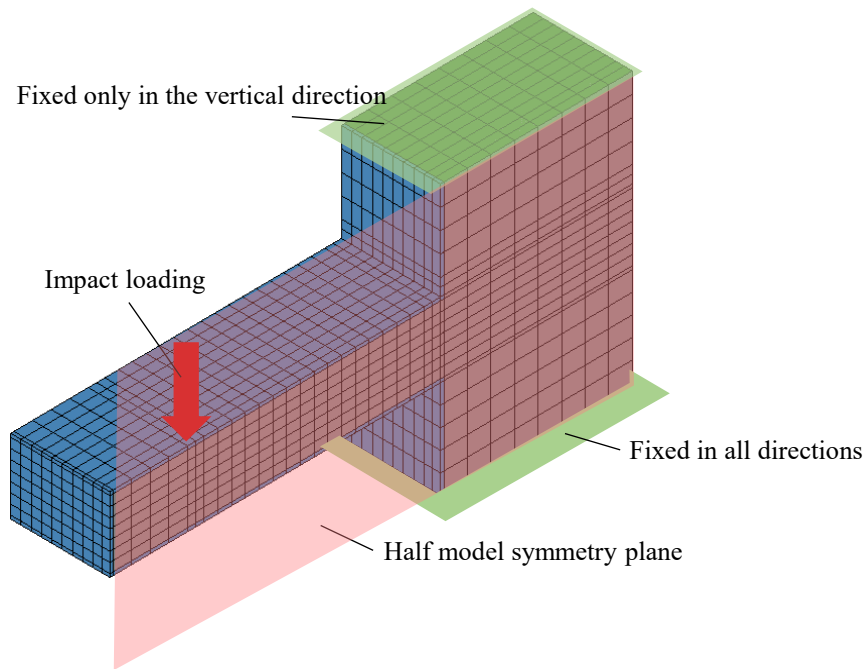
169   direction.

Figure 3.8 Boundary conditions

170

171   When impact analysis is conducted using finite element modeling (FEM), the impactor and the object

172   to be impacted are modeled using finite elements, and the phenomenon is generally reproduced by solving

173   a dynamic contact problem. However, numerical analysis of contact problems is computationally expensive,

174   especially for the present analysis, which requires solving repeated impact loads with more than 10 impacts.

175   Therefore, in this analysis, we adopted the method of directly inputting the impact load to the impact surface

176   of the object to be impacted. Figure 3.9 shows the actual impact load input in the repeated impact analysis.

177   First, the input load for the first impact was created by approximating the impact force waveform

178   obtained from the experiment with a figure consisting of an isosceles triangle and a rectangle. Next, the

179   input load waveform for the second and subsequent impacts was created by assuming that the impact

180   duration was the same as the first impact, and adjusting only the impact force so that the impulse was equal

181   because there were no experimental results. The impulse was obtained by multiplying the change in velocity

182   of weight dropped freely from a given height until it stopped after impact(see Equation (3.10)). The increase

183   in the height of the falling weight due to the residual displacement of the RC beam was added to the

184   prescribed height. In this analysis, the number of impacts was set to 14 to carry out the analysis until the

185   maximum displacement of the uncovered case reached the terminal displacement obtained in the

186   experiment.

187
$$I = m \times (v_1 - v_0) \tag{3.10}$$

188   where I is the impulse received by the impacted object (kg m/s), m is the mass of the dropped weight

189   (kg), v_0 is the velocity immediately before the impact (m/s), and v_1 is the velocity immediately after the
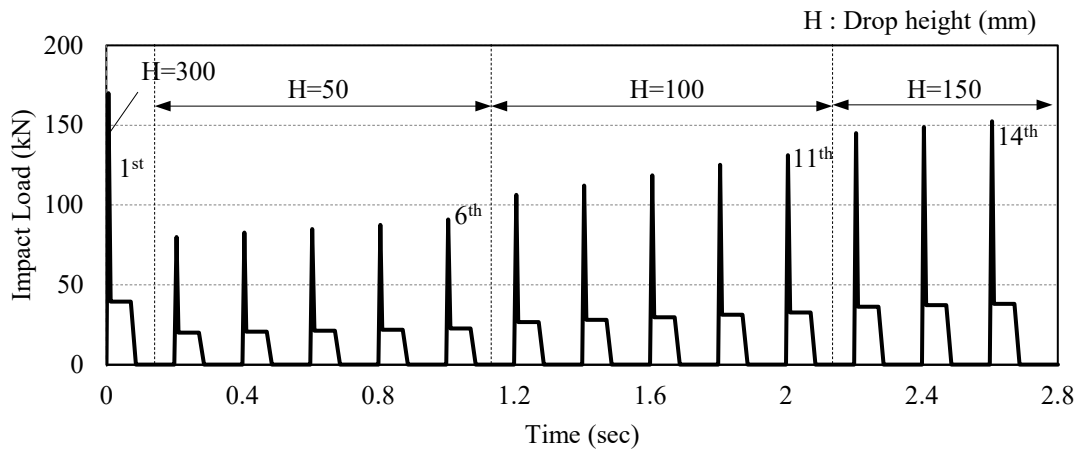
190   impact (m/s).

Figure 3.9 Input load waveform set for repeated impact analysis

191

3.4   <u>Analysis method</u>

193   The FE software DIANA 10.5 was used for this analysis. The Newmark β method (β = 0.25) was used

194   for the time integration method. Rayleigh attenuation is assumed. Equations (3.11) and (3.12) show the

195   equations for the Rayleigh attenuation parameters α and β, where ω_1 and ω_2 are the primary and

196   secondary frequencies, respectively, and h_1 and h_2 are the critical attenuations (= 5%) corresponding to

197   each mode.

198
$$\beta = 2(\omega_1 h_1 - \omega_2 h_2)/\omega_1^2 - \omega_2^2 \qquad (3.11)$$

199
$$\alpha = 2\omega_1 h_1 - \beta \omega_1^2 \qquad (3.12)$$

200

201   **3.5**   **Analysis result and discussion**

202   **3.5.1**   **Comparison of analytical and experimental results**

203   Figure 3.10 shows a comparison of the experiment results and analysis results for the relationship

204   between the number of impacts and maximum displacement. There was no significant influence of polyurea

205   resin on the maximum displacement at the first impact; however, it was possible to reproduce the tendency

206   of the displacement difference to increase gradually with the number of loads.

207   Figure 3.10 shows that the analysis value is smaller than the experimental value after the 7th impact,

208   and this difference increases as the number of impacts increases. One of the main reasons for this is that the

209   impact analysis does not consider the rebound of a falling weight that occurred in the impact test. In fact,

210   the falling weight bounced with each impact test, and damage due to multiple collisions accumulated on

211   the test piece.

212   Figure 3.11 shows the strain distribution of the main reinforcing bars at the time of the 12th and 14th

213   impacts and is divided into three layers by shades of black. The darkest black color shows reinforcing bars

214   that have reached the rupture strain, and the next darkest shade shows the reinforcing bars that have reached

215   the yield strain. According to this figure, for the model without polyurea coating, the outermost main rebar

216   ruptured at the 12th impact, and the second adjacent main rebar ruptured at the 14th impact. Conversely, for

217   the model with polyurea coating, no ruptures of the main reinforcing bar were observed even at the 14th

218   impact. According to the experiment results, five reinforcing bars of the specimen without polyurea coating

219   ruptured and collapsed rapidly at the 11th impact in the experiment, whereas in the analysis the reinforcing

220   bars on the outside of the specimen without polyurea coating collapsed after the 12th impact. Because of

221   the difference in the number of ruptured reinforcing bars and the number of impacts until the reinforcing

222   bars ruptured, the maximum displacement of the analysis result shows a gradual increase, as shown in

223   Figure 3.10. From these results, it was possible to reproduce the same tendency as in the experiment results;

224   for example, the fracture can be suppressed by coating with polyurea resin, and the maximum displacement

225   increases with the fracture of the reinforcing bar.

226   The green line in the Figure 3.10 shows the displacement at the loading point when the main reinforcing

227   bar reaches the rupturing strain under the static load condition on the cantilever. In both the impact

228   experiment and the impact analysis, the fracture of the reinforcing bar was confirmed when the

229   displacement exceeded the level of the green line in the figure. The displacement of the specimen with

230   polyurea coating was below this level even at the 15th impact, and thus the reinforcing bar was considered

231   not to have ruptured yet. Therefore, results show that the coating effect of polyurea resin can increase the

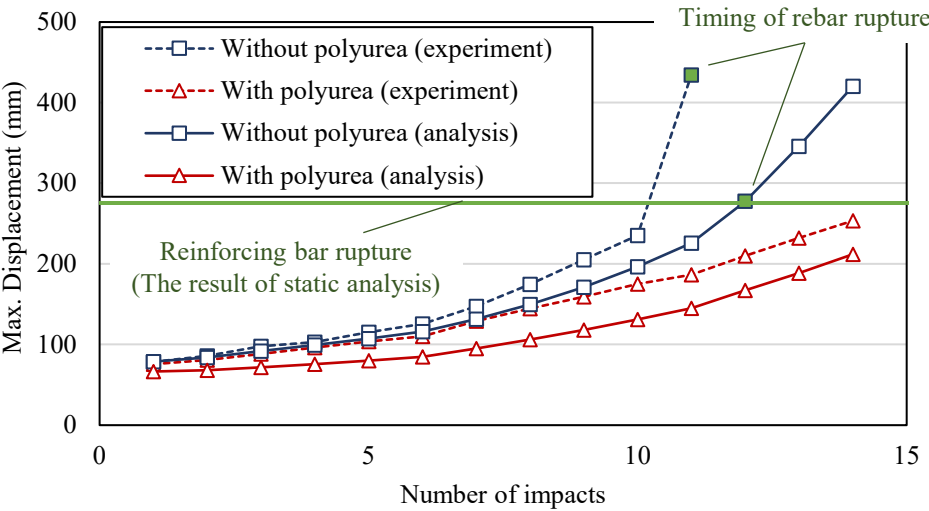232   number of impacts until the rupturing of the reinforcing bar by approximately five.

233

Figure 3.10 Comparison of the experiment results and analysis results for the relationship between

number of loads and maximum displacement

A rebar ruptured

$\varepsilon_{su} = 0.18$

$\varepsilon_y = 0.002$

(a) Without polyurea coating (12 times)　　(b) With polyurea coating (12 times)

Two rebars ruptured

$\varepsilon_{su} = 0.18$

$\varepsilon_y = 0.002$

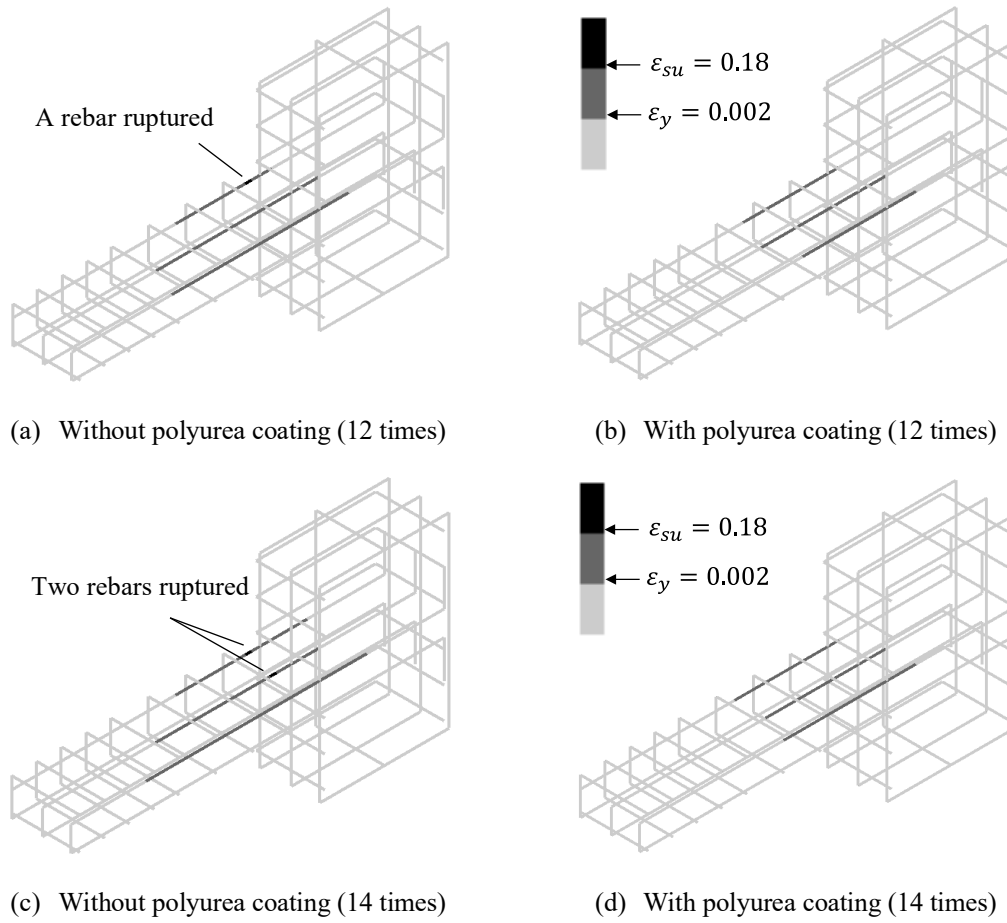(c) Without polyurea coating (14 times)　　(d) With polyurea coating (14 times)

Figure 3.11 Strain distribution of the main reinforcing bars

234

235   **3.5.2   Damage condition of polyurea resin**

236   Figure 3.12 shows the equivalent stress distribution of the polyurea resin at the 14th impact. The tensile

237   stress is particularly concentrated on the polyurea resin at the fixed end of the cantilever beam. Figure 3.13

238   shows the maximum principal strain distribution of the polyurea resin at the 14th impact. From this figure,

239   it can be seen that the polyurea resin has approximately 30% strain, and there is still a margin in its

240   elongation performance. Therefore, it is confirmed that the proposed analysis shows the same tendency as

241   in the experiment, that the polyurea resin prevents tensile failure at the fixed end of the cantilever.
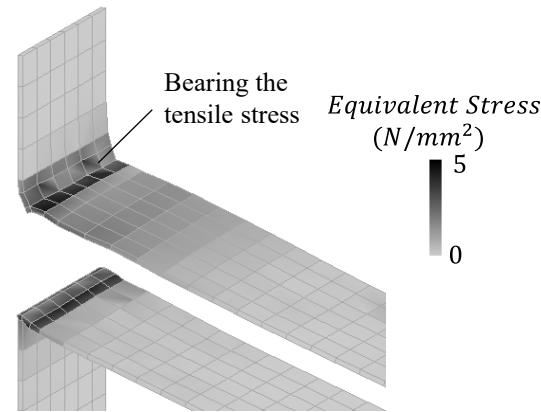
242

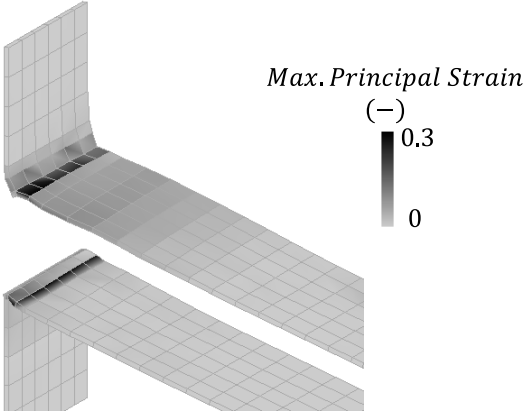Figure 3.12 Equivalent stress distribution of the   Figure 3.13 Maximum principal strain distribution

polyurea resin at the 14th impact   of the polyurea resin at the 14th impact.

243

244 **4** **Push-off test and FEM analysis of polyurea resin**

245 **4.1** **Test outline**

246   To evaluate the performance of polyurea resin at preventing peeling off, a test was conducted according

247 to the JSCE standard (JSCE-K 533-2010) and tried to reproduce the test using FEM analysis. The test was

248 carried out by three specimens of a rectangular (400×600×60 mm) concrete member, as shown in Figure

249 4.1. Each specimen was cored to a depth of 55 mm in a circular shape with a diameter of 100 mm, and the

250 back was coated with polyurea resin to a thickness of 1.5 mm. In the tests, the core was first loaded until

251 the core (remaining concrete with a thickness of 5 mm) failed, and then loaded under displacement control

252 up to a maximum displacement of 50 mm. At displacement points of 10, 20, and 30 mm, the range of resin

253 peeling was marked, and the ability of the polyurea resin layer to prevent peeling was confirmed.
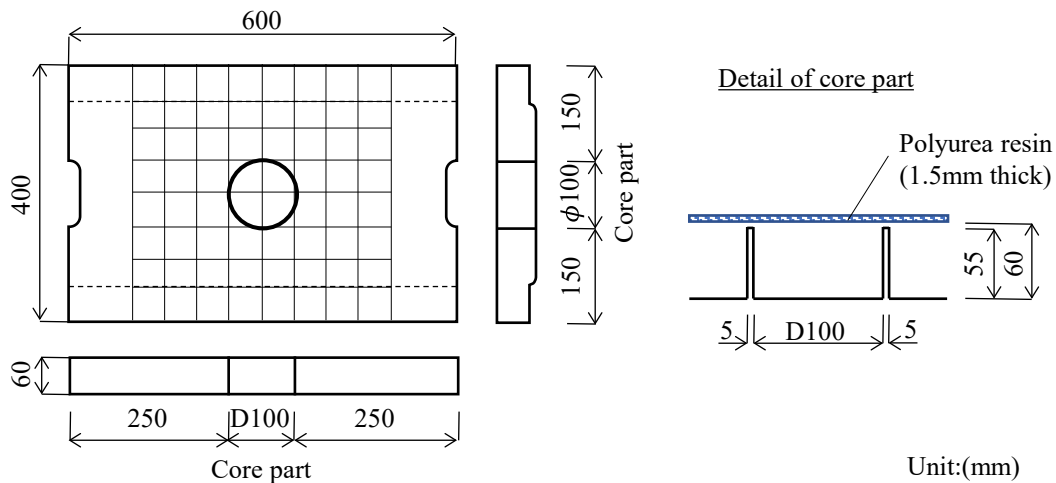
Figure 4.1 Schematic diagram of the test specimen

254   Figure 4.2 shows the load-displacement relationship. The range highlighted in yellow, which indicates

255 a push-off displacement of more than 10 mm and a push-off resistance force of more than 1.5 kN, is the

256 acceptance range defined by the standards for verification of peeling prevention performance of the 3

257 Japanese highway companies (East, Central and West Nippon Expressway Company Limited). From this

258　　figure, it was confirmed that the average of the maximum loads was 2.3kN, which was within the acceptable

259　　displacement range and exhibited sufficient performance to prevent peeling. The condition after the test is

260　　shown in Photo 4.1 (a), (b), and (c). The circular lines in the photos indicate the range of polyurea resin

261　　peeling off at 10, 20, 30, and 50mm displacement, respectively. The peeling area expands as the push-off

262　　displacement increases, while the polyurea resin peels off from the concrete matrix and functions as a film

263　　covering the back surface. Figure 4.3 shows a schematic diagram showing the expansion of the peeling area
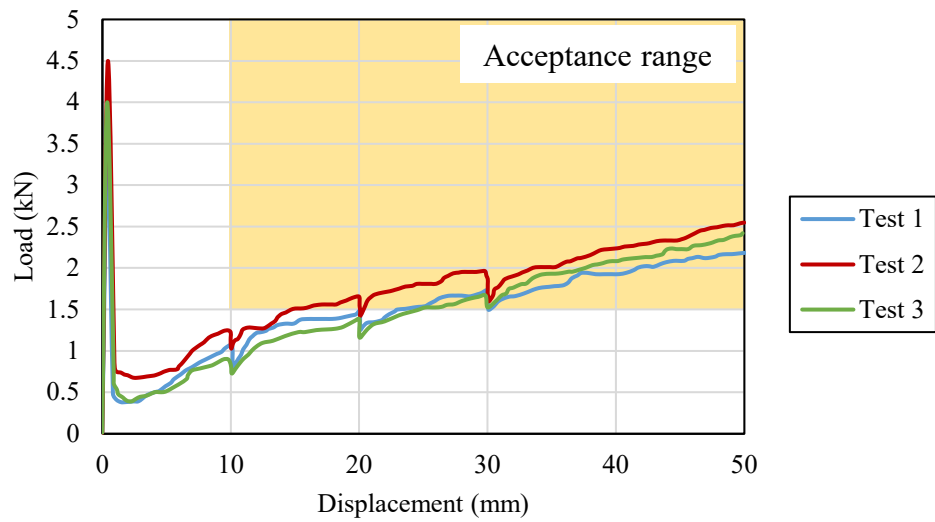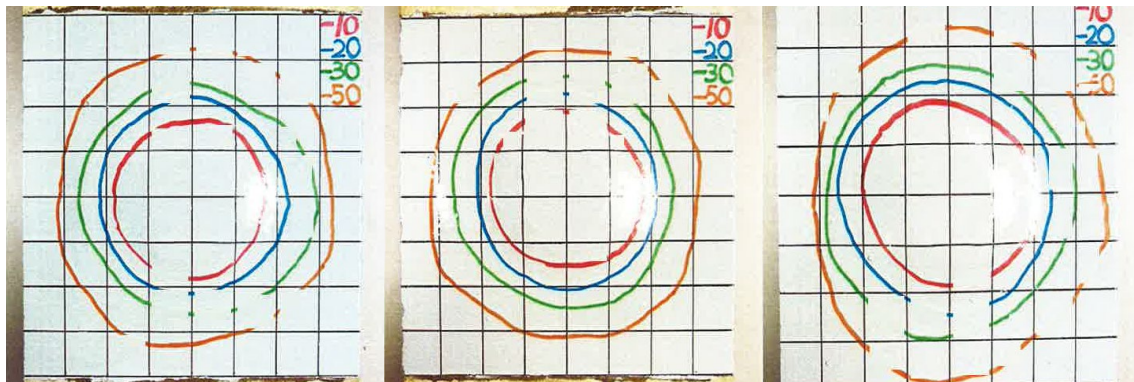
264　　by pushing out.

Figure 4.2 Load-displacement relationship

(a) Test 1   (b) Test 2   (c) Test 3

Photo 4.1 Condition of the specimens after the test

Push-off

A core of concrete   Concrete plate
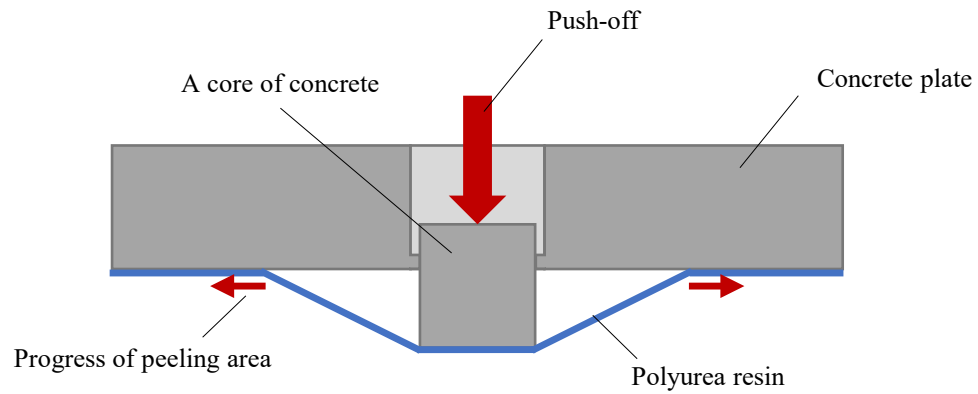
Progress of peeling area

Polyurea resin

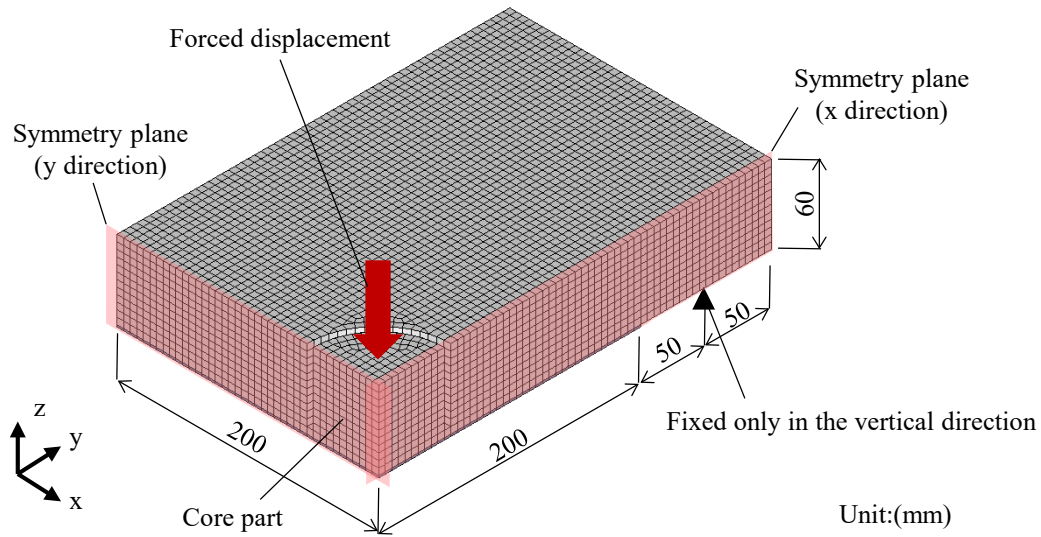Figure 4.3 Schematic diagram showing the expansion of the peeling area

Figure 4.4 1/4 Finite element model for concrete plate

Table 4.1 Physical properties

Material	Mass density [kg/m³]	Young's modulus [kN/mm^2]	Poisson's ratio	Strength [N/mm^2]
Steel	7853	206	0.3	394.1(yield)
Concrete	2160	18.63	0.19	36.0(compressive), 3.6(tensile)
Polyurea resin	1000	0.11	0.26	24.0

266

267 **4.2   FEM analysis result**

268   Figure 4.4 shows the 1/4 FE model. The failure of the remaining 5 mm concrete layer in the central core

269 is not considered in this analysis. The physical properties of each material are shown in Table 4.1. Figure

270 4.5 shows a comparison between the test and analysis based on the load-displacement relationship. Because

271 the failure of the concrete at the core joint was not considered, the analysis did not show a sudden increase

272 in the initial load condition; however, results after that were mostly able to reproduce the test.

273   Figure 4.6 shows the relative displacement contours in the normal direction of the interface element

274   located between the polyurea resin and the concrete. The lower limit of the contour is set to the relative

275   displacement at the time of adhesion failure, and the area contoured in colors other than purple indicates

276   the area where the polyurea resin has peeled off. The model is able to reproduce the gradual expansion of

277   the peeling area as the pushing displacement increases. Table 4.2 shows the comparison of the radius r

278   (mm) of the peeling area between the test and analysis. The radius r of the peeling area in the test was

279   measured from Photo 4.1 (a), (b), and (c), and averaged over all three specimens. Comparing the results of

280   the test and the analysis, the radius of the peeling area was nearly identical.
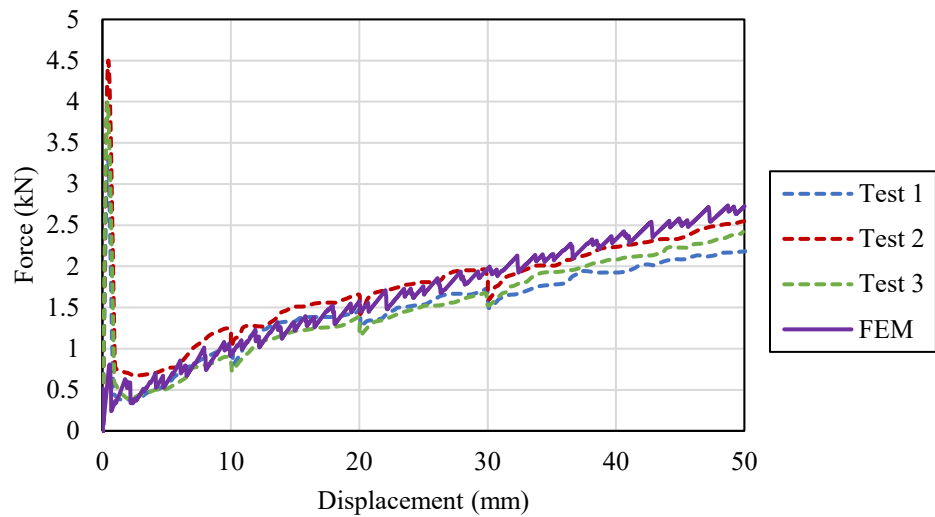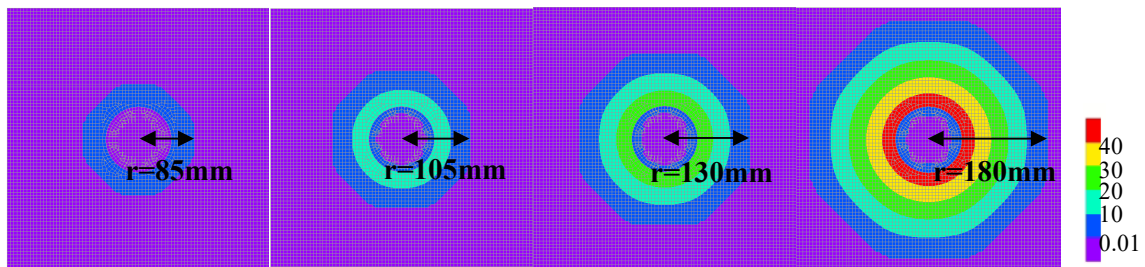
281

Figure 4.5 Load-displacement relationship

(a) Disp. 10 mm   (b) Disp. 20 mm   (c) Disp. 30 mm   (d) Disp. 50 mm

Figure 4.6 Relative displacement contours in the normal direction

Table 4.2 Comparison of radius of peeling area between test and analysis

Displacement (mm)	Radius of peeling area : r (mm)				
	Test 1	Test 2	Test 3	Average	FEM
10	80	80	90	83	85
20	115	110	115	113	105
30	125	125	145	132	130
50	160	160	175	165	180

282

283 **5   Medium-speed repeated impact of RC slab**

284

285   To examine the response of RC members coated on the back side with polyurea resin to medium-

286 velocity impact loads, a repeated lateral impact test was conducted on the RC slab.

287

288   **5.1   Experiment outline**

289   Figure 5.1 shows a schematic diagram of the test specimen. The test specimen is a square plate with

290 dimensions of 600 mm (length)×600 mm (width) ×90 mm (height). D6(SD295A) reinforcing bars were

291 used for the tensile side, with five bars in each direction at 125 mm intervals. A 2 mm thickness of polyurea

292 resin was applied to the back of the specimen. The tests were conducted using a horizontal impact testing

293 machine. Figure 5.2 shows the flying object, Photo 5.1 shows the horizontal impact test device, and Photo

294 5.2 shows the supporting condition. A flying object with a diameter of 50 mm, a mass of 3 kg, and repeatedly

295 loaded at a constant speed of 10 m/sec on a test specimen supported on two sides between the upper and
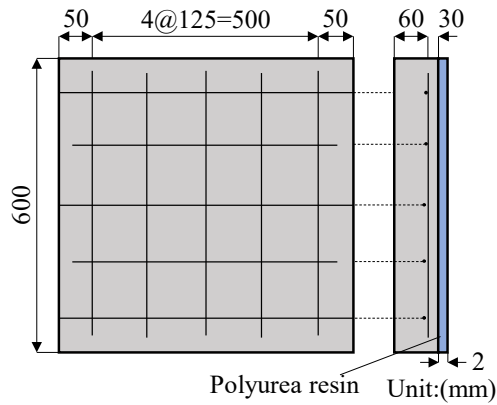
296 lower fulcrums.
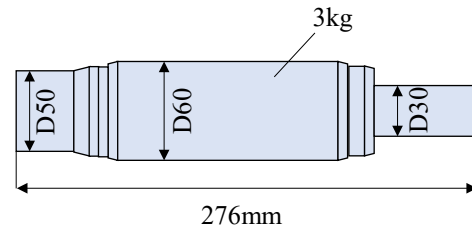
Figure 5.1 Schematic diagram of the test specimen

Figure 5.2 Shape of the flying object
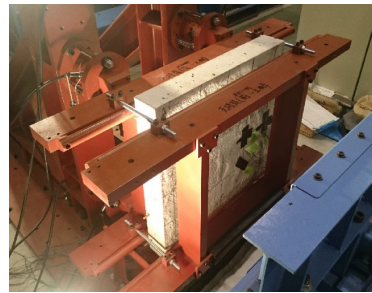
297

Photo 5.1 Horizontal impact test device

Photo 5.2 Supporting condition

298

299   A high-speed video camera with a resolution of 260,000 pixels (512×512) and a recording speed of

300   10,000 frames per second was used, and the time history of the displacement of the flying object was

301   calculated by analyzing the obtained continuous images. Velocity and acceleration were calculated by

302   differentiating the time history of the displacement. The impact load was calculated indirectly by

303   multiplying this acceleration by the mass of the flying object.

304

305   **5.2   Experimental result**

306   Table 5.1 shows the failure status of the front and back sides of the specimens after the final loading.

307   It was determined that the specimen without polyurea failed at the 5th loading when the concrete
308   corresponding to the covering thickness of the reinforcing bar peeled off from the back side. For the
309   specimen with polyurea coating, back side peeling occurred at the 6th loading, however the polyurea resin
310   prevented the concrete pieces from scattering, and the test was terminated at the 13th loading. The failure
311   mode of the test specimen was penetration from front side and slight cracking of the polyurea resin. Thus,
312   by coating the polyurea resin on the back side, the effect of preventing the concrete pieces from scattering
313   was confirmed.

Table 5.1 Failure status of the front and back sides of the specimens

Case	RC slab		RC slab with polyurea resin on the back surface	
	Front side	Back side	Front side	Back side
Pictures				
Fracture form	Back side peeling of concrete pieces		Penetration fracture of front concrete & crack fracture of polyurea	
Number of impacts	5		13	
Peeling area on back side	75000mm²		87500mm²	

314

315   Figures-5.3 (a) and (b) show the impact loads at the 1st and 5th loads, which were measured by analyzing
316   the images captured by the high-speed video camera. Figure 5.4 shows the relationship between the
317   maximum impact force and the number of impacts. In Figure 5.4, when comparing the maximum impact
318   force at the 1st and 5th impacts, the specimen without polyurea showed a significant decrease at the 5th
319   impact, which was approximately 55% less than the 1st impact due to the back side peeling which reduced

320   the stiffness of the member. In contrast, the maximum impact force of the specimen with polyurea coating

321   decreased by 34% at the 5th impact and 43% at the 6th impact. These results show that the back side coating

322   of polyurea resin not only prevented the scattering of concrete pieces that peeled off the back side, but also

323   suppressed the reduction in stiffness when the back side peeled off.
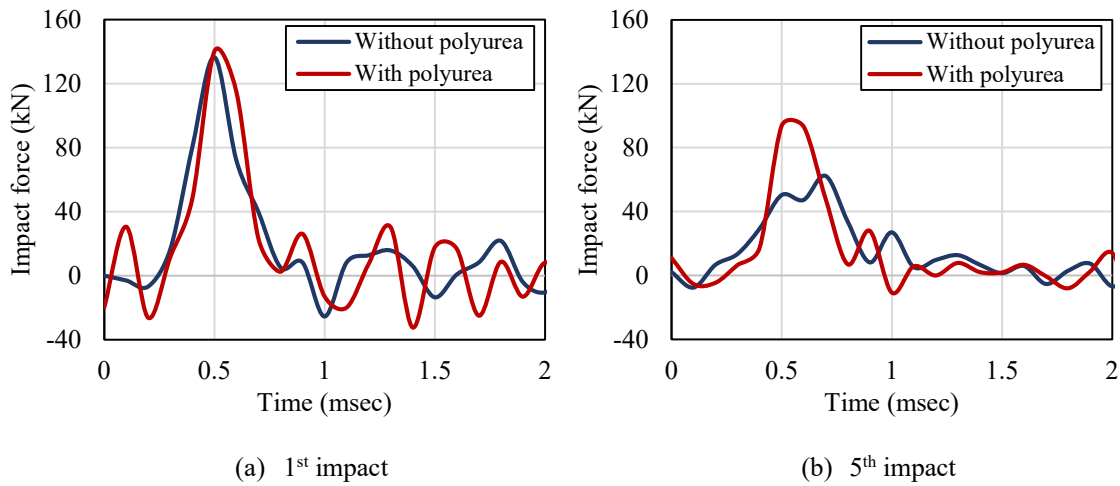

(a) 1st impact   (b) 5th impact

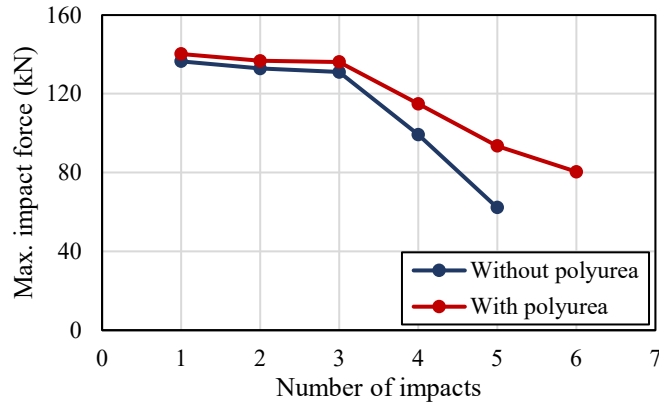Figure 5.3 Impact loads of the flying object

Figure 5.4 Relationship between maximum impact force and number of impacts

324

325   **6**   **Numerical simulations for medium-speed repeated impact test of RC slab**

326

327   This section numerically evaluate the effect of polyurea resin coating on the prevention of scattering

328 and discusses the results. However, this analysis is still in the basic study stage, and the evaluation of the

329 coating effect is limited to a relative comparison.

330

331   **6.1**   **Finite element model and boundary condition**

332   Figures 6.1 (a) and (b) show a schematic diagram of the model. The dimensions of the specimens were

333 the same as the tests, and the reinforcing bars were modeled using truss elements, while the others were

334 modeled using three-dimensional solid elements. As for the support conditions, the model was supported

335 on two sides as shown in Figure 6.1 (b). For the loading conditions, repeated impact loading was applied

336 by inputting the impact load. The number of loadings was the same as in the experiment. Figure 6.2 shows

337 the impact load input for this analysis. The impact load was created by approximating the impact load wave

338 of the flying object (Figure 5.3) as a triangular wave. In this analysis, only the concrete elements of the

339 loading surface were assumed to be without compressive softening. Because, if the compressive failure of

340 the loading surface element were considered, impact load would be input to the crushed element, and it

341 would not be transferred to the entire model. To prevent this problem and impose more severe conditions

342 on the backside peeling, the same impact load as the 4th impact was input repeatedly after the 5th impact.

343

Coating thickness: 2mm

(a) 1/2 Finite Element model for RC slab

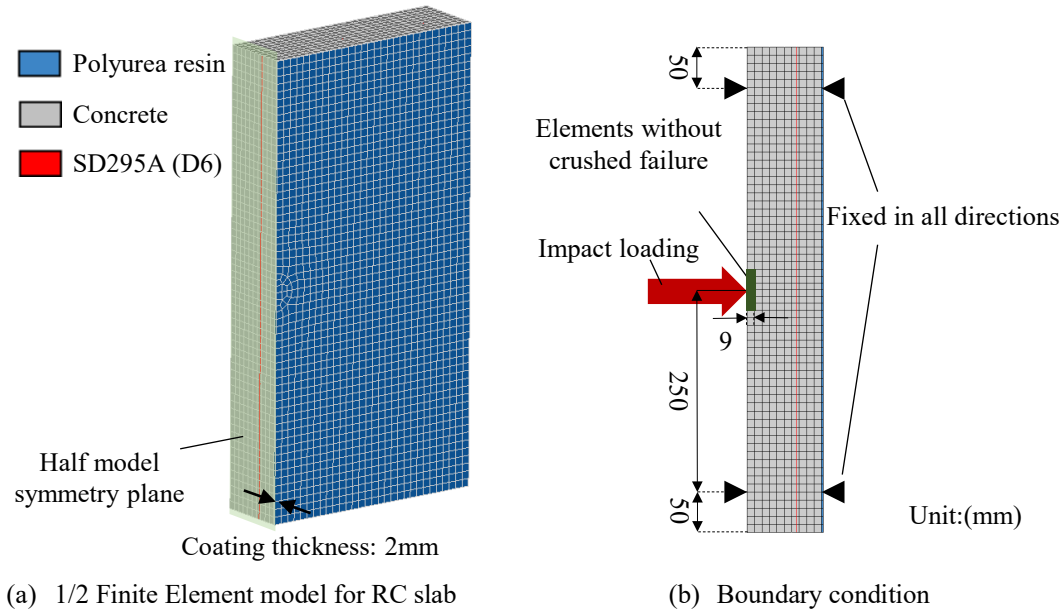(b) Boundary condition

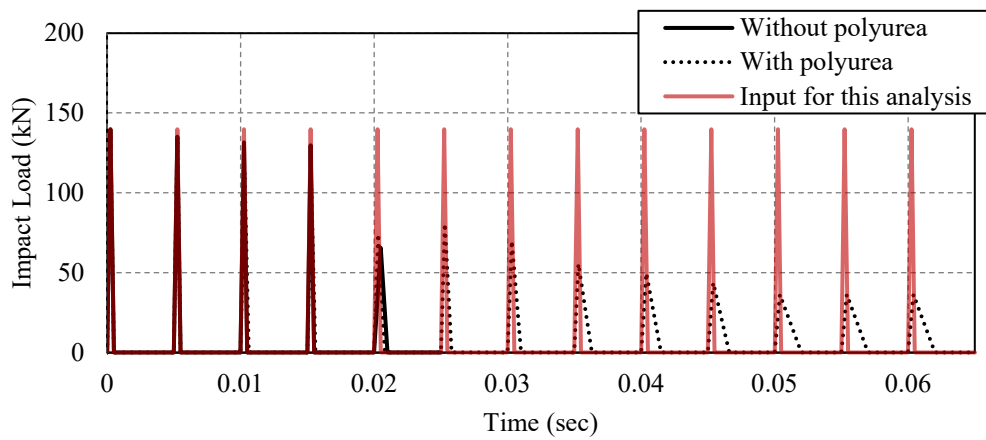Figure 6.1 Schematic diagram of the model

Figure 6.2 Impact load input for this analysis

6.2 Physical properties and analysis method

Table 6.2 shows the physical properties of each material. The material models for the various materials and interfaces are the same as those described in Section 3.2. and the analysis method is the same as that described in Section 3.4.

Table 6.2 Physical properties

Material	Mass density [kg/m³]	Young's modulus [kN/mm²]	Poisson's ratio	Strength [N/mm²]
Steel	7850	200	0.3	295(yield)
Concrete	2320	22.9	0.2	33.3(compressive), 2.38(tensile)
Polyurea resin	1000	0.11	0.26	24.0

348

349 ## 6.3   **Analysis results and discussion**

350   Table 6.3 shows the maximum principal strain distributions for the back side of RC slabs with and

351 without polyurea coating and the back side of polyurea resin. Comparing the strain distributions of the RC

352 slab with and without polyurea resin coating, there is no significant difference between them. In addition,

353 in the test, back side peeling occurred at almost the same number of impacts in both cases. Thus, it can be

354 concluded that the back side coating of polyurea resin has almost no effect on preventing cracking and

355 peeling of the back side. In the strain of the model without polyurea at the 5th impact shown in Table 6.3, it

356 is assumed that back side delamination occurs as in the test. Comparing the strain distribution of the model

357 without polyurea at the 5th impact and that of the model with polyurea at the 13th loading, it could be seen

358 that the latter has developed more damage. However, the strain distribution on the back side of the polyurea

359 resin showed that the maximum strain at the 13th impact was approximately 0.01, which was not far from

360 the ultimate strain of 3.5, indicating that there was still a margin of elongation performance. In conclusion,

361 it can be indirectly expressed that the coating of polyurea resin on the back side of the RC slab can prevent

362 the scattering of concrete flakes even if significant damage occurs to the back side of concrete, because it

363 is covered with sound polyurea resin (Figure 6.3).

Table 6.3 Maximum principal strain distributions for the back side of RC slabs with and without

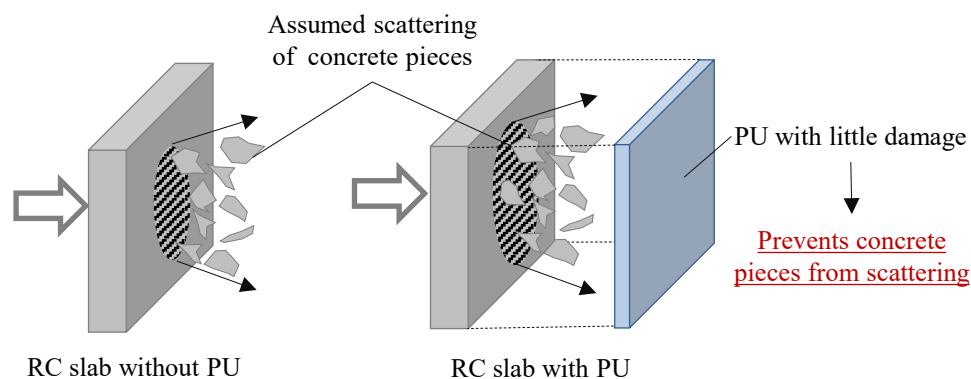polyurea coating, and the back side of polyurea resin

Number of impacts		1st	5th	8th	13th
Without polyurea	Back side of concrete				2,500μ 1,000μ 100μ 0μ
With polyurea	Back side of concrete				
	Back side of polyurea				

Assumed scattering
of concrete pieces

PU with little damage

↓

Prevents concrete
pieces from scattering

RC slab without PU   RC slab with PU
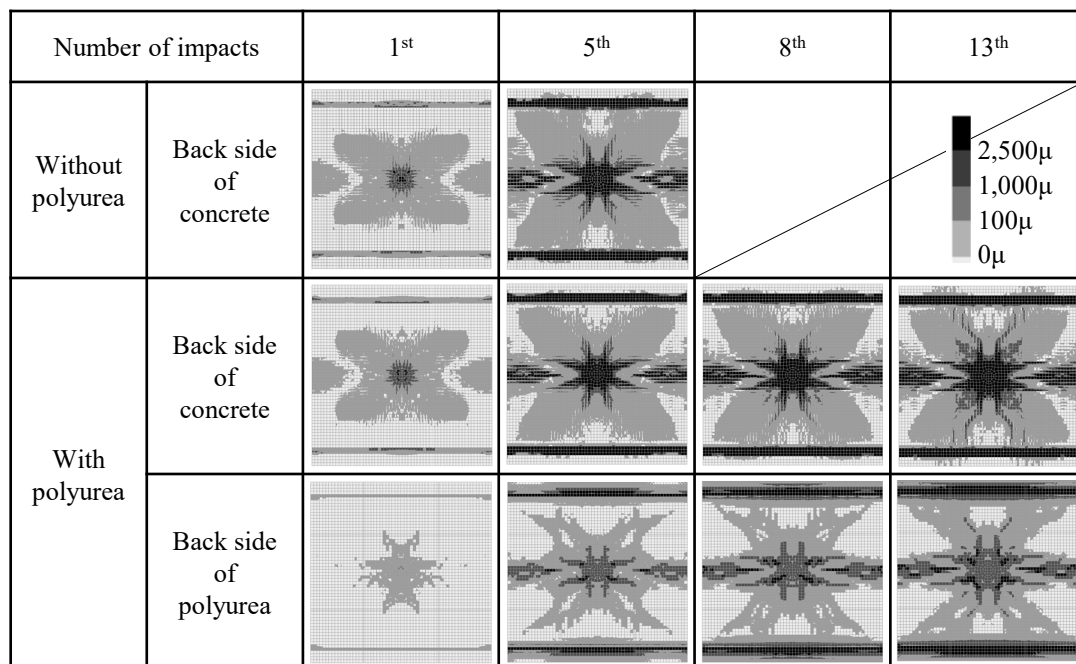
Figure 6.3 Schematic diagram of the mechanism by which polyurea resin prevents the scattering effect

364

6.4   Effect of polyurea resin coating in case of considering penetration fracture

366   In the medium-velocity repeated collision test, it was confirmed that the resin-coated test piece had

367 penetrating fracture from front side that reached the internal reinforcing bar, but the analysis in the previous

368 section did not consider it. Therefore, it is highly possible that the load bearing performance is

369 overestimated. Therefore, we modeled penetrating fracture of the front side in FEM analysis and considered

370 the effect of polyurea resin on the backside peeling prevention effect.

371 ### 6.4.1 Modeling penetration fracture

372 Figure 6.4 shows the outline of the modeling of penetrating fracture. The penetrating fracture was

373 reproduced by sequentially deleting the concrete elements that were judged to be crushed and reducing the

374 thickness of the RC plate. In addition, the loading surface element is deleted in layer units (when the average

375 minimum principal strain of the in-layer element reaches 0.01) in order to keep the loading surface is flat.

376 However, if the penetrating fracture reached to the reinforcing bar, it was assumed that the penetration

377 would not proceed furthermore.
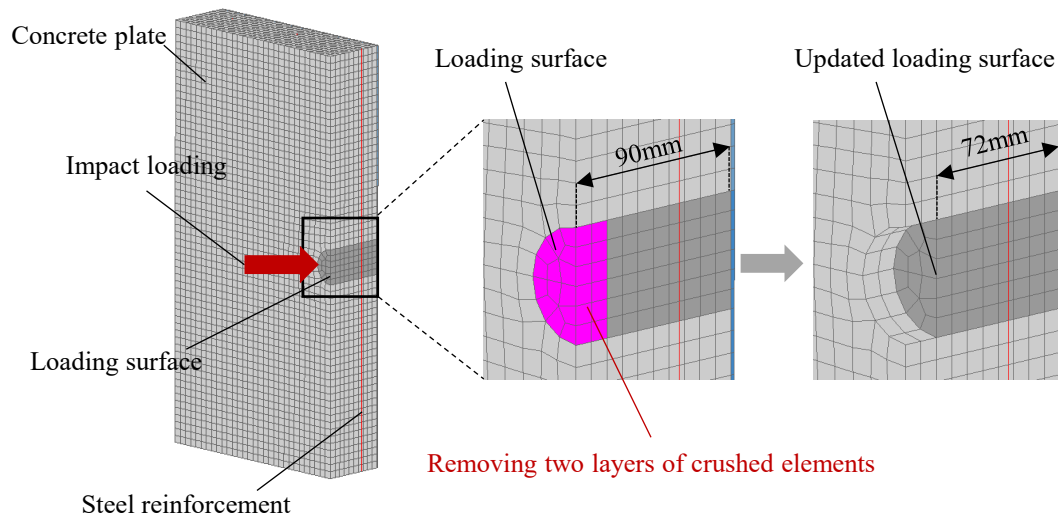
Figure 6.4 The outline of the modeling of penetrating fracture

378

379 ### 6.4.2 Analysis result

380 Figure 6.5 shows the remaining thickness of the RC plate for each number of loads. From this figure,

381 as the number of loads increased, the plate thickness decreased with the progress of penetrating fracture,

382 and under this loading conditions, the penetration reached to the element adjacent to the reinforcing bar at

383 the 9th shot.

384   Table 6.4 shows the maximum principal strain of the back surface of RC slab and the polyurea resin. It

385   was clearly shown that the damage was locally predominant compared to the previous results. Compared

386   to the maximum principal strain of the resin at 13th collision, the maximum strain was 0.029, which was

387   2.9 times larger than that of the maximum strain without compressive fracture assumption. Therefore, even

388   when considering the compressive fracture of concrete, the high backside peeling prevention effect of

389   polyurea resin was recognized.

390

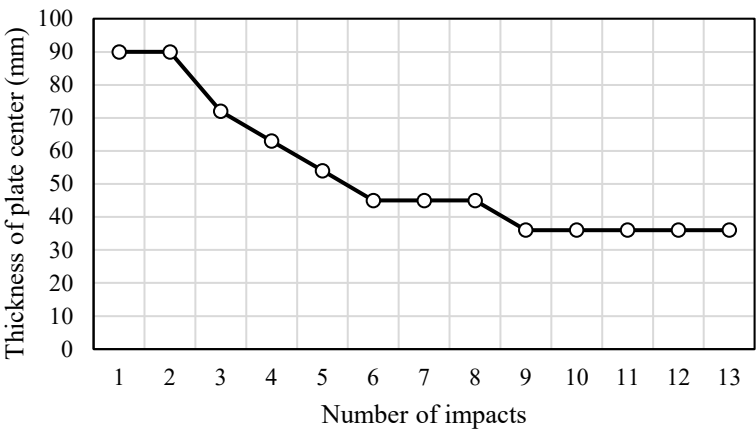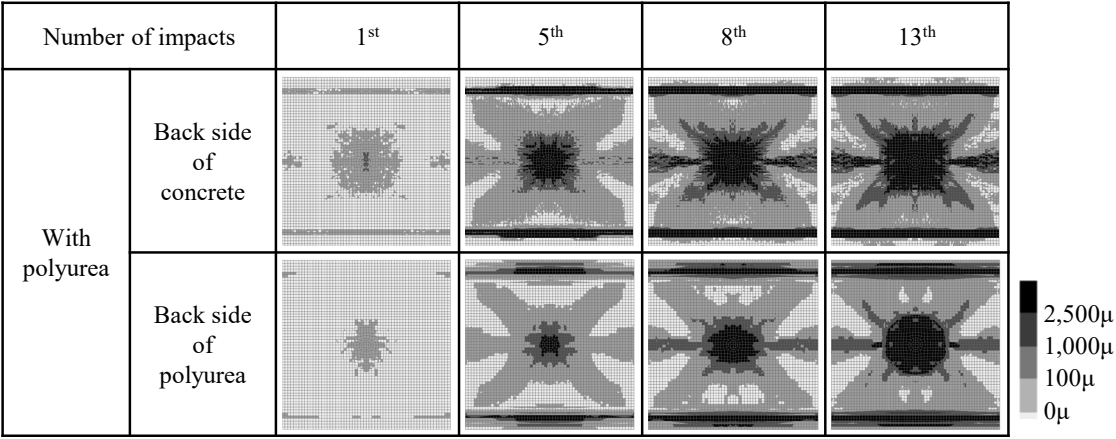Figure 6.5 The remaining thickness of the RC plate for each number of loads

Table 6.4 Maximum principal strain distributions for the back side of RC slabs

with and without polyurea coating, and the back side of polyurea resin

Number of impacts		1st	5th	8th	13th
With polyurea	Back side of concrete				
	Back side of polyurea				

2,500μ
1,000μ
100μ
0μ

391

392 **7   <u>Conclusion</u>**

393

394   In this study, the impact resistance performance of RC members coated with polyurea resin under low-

395   speed and medium-speed impact loads was examined through experiments and numerical simulations. The

396   results of this study are summarized as follows:

397   1)   According to the low-speed repeated impact test conducted on the RC cantilever beam, there was no

398   significant effect under the first impact. However, when the number of impacts increased, the

399   strengthening effect of the polyurea resin was confirmed. For example, a cross-linking effect between

400   the upper surface of the cantilever and the pier surface of the fixed support was observed. Furthermore,

401   the effect of preventing the concrete pieces from peeling off on the compression side of the cantilever

402   was also confirmed. Thus, it was confirmed that the polyurea resin layer can improve the energy

403   absorption capacity of RC structural members under impact loads.

404   2)   When a medium-speed repeated impact test was performed on the RC slab coated with polyurea resin

405   on the back side, it was found that the input energy required for fracture was significantly increased

406   as compared to the case of low-speed impact. In addition, by coating the back side of the RC slab, not

407   only the effect of preventing the scattering of concrete pieces but also the effect of suppressing the

408   decrease in rigidity of the entire member was confirmed.

409   3)   FE analysis of both types of impact experiments was performed, and the following effects were

410   reproduced. The impact resistance performance of the RC beam was improved using a polyurea resin

411   layer. In addition, although cracking and back side peeling of the concrete slab cannot be suppressed,

412   scattering of the peeled pieces can be prevented by coating them with polyurea resin.

413

414 **References**

415 [1] Yi J, Boyce MC, Lee GF, et al. (2006)

416 **Large deformation rate-dependent stress-strain behavior of polyurea and polyurethanes**

417 *The International Journal for the Science and Technology of Polymers* 47(1): 319-329.

418 https://doi.org/10.1016/j.polymer.2005.10.107

419 [2] Roland CM, Twigg JN, Vu Y, et al. (2007)

420 **High strain rate mechanical behavior of polyurea**

421 *The International Journal for the Science and Technology of Polymers* 48(2): 574-578.

422 https://doi.org/10.2208/jscejmcs.72.146

423 [3] Sarva SS, Deschanel S, Boyce MC, et al. (2007)

424 **Stress-strain behavior of a polyurea and a polyurethane from low to high strain rates**

425 *The International Journal for the Science and Technology of Polymers* 48(8): 2208-2213.

426 https://doi.org/10.1016/j.polymer.2007.02.058

427 [4] Shim J, Mohr D (2009)

428 **Using split Hopkinson pressure bars to perform large strain compression tests on polyurea at**

429 **low, intermediate and high strain rates**

430 *International Journal of Impact Engineering* 36(9): 1116-1127.

431 https://doi.org/10.1016/j.ijimpeng.2008.12.010

432 [5] Youssef G, Gupta V (2012)

433 **Dynamic tensile strength of polyurea**

434 *Journal of Materials Research* 27(02) 494-499.

435 https://doi.org/10.1557/jmr.2011.405

436 [6] Raman SN, Ngo T, Lu J, et al. (2013)

437 **Experimental investigation on the tensile behavior of polyurea at high strain rates**

438 *Materials & Design* 50: 124-129.

439 https://doi.org/10.1016/j.matdes.2013.02.063

440 [7] Amini MR, Isaacs JB, Nemat-Nasser S (2010)

441 **Experimental investigation of response of monolithic and bilayer plates to impulsive loads**

442 *International Journal of Impact Engineering* 37(1): 82-89

443 https://doi.org/10.1016/j.ijimpeng.2009.04.002

444 [8] Samiee A, Amirkhizi AV, Nemat-Nasser S (2013)

445 **Numerical study of the effect of polyurea on the performance of steel plates under blast loads**

446 *Mechanics of Material* 64: 1-10.

447 https://doi.org/10.1016/j.mechmat.2013.03.008

448 [9] Jiang Y, Zhang B, Wei J, et al. (2019)

449 **Study on the impact resistance of polyurea-steel composite plates to low velocity impact**

450 *International Journal of Impact Engineering* 133: 103357.

451 https://doi.org/10.1016/j.ijimpeng.2019.103357

452 [10] McShane GJ, Stewart C, Aronson MT, et al. (2008)

453 **Dynamic rupture of polymer–metal bilayer plates**

454 *International Journal of Solids and Structures* 45: 4407-4426.

455 https://doi.org/10.1016/j.ijsolstr.2008.03.017

456 [11] Takeuchi K, Kamiya T, Nomura T, et al. (2015)

457 **Experimental study on the impact resistance of steel box coated with polyurea resin**

458 *Journal of Structural Engineering* A 61: 851-858.

459 [12] Ichino H, Nagata M, Beppu M, et al. (2016)

460 **Effects of Reinforcing Back Surface of Concrete Plates on Local Damage Caused by Explosive**

461 **load**

462   *Journal of Japan Society of Civil Engineers, Ser. E2 (Materials and Concrete Structures)* 72(2): 146-

463   164.

464   [13] Chen Y, Wang B, Zhang B, et al. (2020)

465   **Polyurea coating for foamed concrete panel: an efficient way to resist explosion**

466   *Defence Technology* 16: 136-149.

467   https://doi.org/10.1016/j.dt.2019.06.010

468   [14] Ha JH, Yi NH, Choi JK, et al. (2011)

469   **Experimental study on hybrid CERP-PU strengthening effect on RC panels under blast loading**

470   *Composite Structures* 93: 2070-2082.

471   https://doi.org/10.1016/j.compstruct.2011.02.014

472   [15] Parniani S., Toutanji H. (2015)

473   **Monotonic and fatigue performance of RC beams strengthened with a polyurea coating system**

474   *Construction and Building Materials* 101: 22-29.

475   https://doi.org/10.1016/j.conbuildmat.2015.10.020

476   [16] Japan Society of Civil Engineering (2012)

477   **Standard Specifications for Concrete Structures-2012, Structural Performance Evaluation**

478   Japan Society of Civil Engineering: Tokyo, Japan,

479   [17] Hordijk DA (1991)

480   **Local Approach to Fatigue of Concrete**

481   PhD thesis, Delft University of Technology, Netherlands

482   [18] Dodd LL, Restrepo-Posada JI. (1995)

483   **Model for Predicting Cyclic Behavior of Reinforcing Steel**

484   *Journal of Structural Engineering* 121(3): 433–445.

485   [19] Shima H., Chou, LL., Okamura H. (1987)

486   **Micro and Macro Models for Bond in Reinforced Concrete**

487   *Journal of the Faculty of Engineering, The University of Tokyo (B)* 39(22): 133–194.

488   [20] Amirkhizi AV, Isaacs J, McGee J, et al. (2006)

489   **An experimentally-based viscoelastic constitutive model for polyurea, including pressure and**

490   **temperature effects**

491   *Philosophical Magazine* 86(36): 5847-5866.

492   https://doi.org/10.1080/14786430600833198

493   [21] Li C, Lua J (2009)

494   **A hyper-viscoelastic constitutive model for polyurea**

495   *Materials Letter* 63(11): 877-880.

496   https://doi.org/10.1016/j.matlet.2009.01.055

497   [22] Zhang X, Wang J, Guo W, et al. (2017)

498   **A bilinear constitutive response for polyureas as a function of temperature, strain rate and**

499   **pressure**

500   *Journal of Applied Polymer Science* 134(35): 45256

501   https://doi.org/10.1002/app.45256